THE ASTROPHYSICAL JOURNAL, 524:831–848, 1999 October 20

AN ABUNDANCE ANALYSIS OF TWO CARBON-RICH PROTO–PLANETARY NEBULAE: IRAS Z02229+6208 AND IRAS 07430+1115

BACHAM E. REDDY,[1,2] ERIC J. BAKKER,[3,4] AND BRUCE J. HRIVNAK[1]
Received 1999 April 6; accepted 1999 June 8

ABSTRACT

In this paper, we present an LTE abundance analysis of two new proto–planetary nebulae, IRAS Z02229+6208 and IRAS 07430+1115, based on high-resolution ($R \approx 55{,}000$) optical echelle spectra. Results show that both stars are metal-poor ([Fe/H] = −0.5) and overabundant in C, N, and *s*-process elements. The average elemental abundances are [C/Fe] = +0.8, [N/Fe] = +1.2, and [*s*-process/Fe] = +1.4 for IRAS Z02229+6208, and [C/Fe] = +0.6, [N/Fe] = +0.4, and [*s*-process/Fe] = +1.6 for IRAS 07430+1115. These abundances suggest that the stars have experienced nucleosynthesis on the asymptotic giant branch (AGB), and the resultant products of CNO, 3α, and *s*-process reactions were brought to the photosphere during shell flashes and deep mixing episodes during the AGB phase of their evolution. Of major significance is the measurement of a high Li abundance in both stars, $\log \epsilon(\mathrm{Li}) \approx 2.3$ and 2.4 for IRAS Z02229+6208 and IRAS 07430+1115, respectively. This may be the result of hot bottom burning, below the deep convective zone. We also present an analysis of the circumstellar molecular (C_2 and CN) and atomic (Na I and K I) absorption spectra of both stars. We derive rotational temperatures, column densities, and envelope expansion velocities using molecular C_2 Phillips and CN Red system bands. The values derived for expansion velocities, 8–14 km s^{-1}, are typical of the values found for post-AGB stars. IRAS 07430+1115 is unusual in that it shows P Cygni–shaped C_2 emission profiles in the spectra of the circumstellar envelope. A minimum distance for IRAS Z02229+6208, determined from interstellar Na I lines, suggests that it is evolved from an intermediate-mass star. Including these two stars, the number of post-AGB stars for which clear C, N, and *s*-process elemental overabundances are found rises to eight. IRAS Z02229+6208 is known to possess the 21 μm emission feature in its mid-infrared spectrum; these results support the idea that all 21 μm emission stars are carbon-rich post-AGB stars.

Subject headings: circumstellar matter — ISM: lines and bands — stars: abundances — stars: AGB and post-AGB

1. INTRODUCTION

The proto–planetary nebula (PPN) phase is one of the important but least understood stages in the evolution of low- and intermediate-mass stars. Objects in this stage are in transition between the asymptotic giant branch (AGB) and planetary nebula (PN) phases. The study of PPNs became active only after the launching of the *Infrared Astronomical Satellite* (*IRAS*) in 1983. Since then many objects have been proposed as PPN or post-AGB candidates based on their infrared colors and follow-up ground-based observations (Parthasarathy & Pottasch 1986; Hrivnak, Kwok, & Volk 1989; Hrivnak 1995; Reddy & Parthasarathy 1996; García-Lario et al. 1997). The general properties of PPNs have been summarized by Kwok (1993) and more recently by Hrivnak (1997).

Analysis of the chemical composition is probably the best tool to ascertain the post-AGB nature of these stars and also to understand both the nucleosynthesis mechanisms during the AGB phase and during the subsequent evolution toward the PN phase. Chemical composition analysis of many bright, high-latitude supergiants, which were previously thought to be post-AGB stars, showed that their large CNO abundances are due not to nucleosynthesis but rather to depletion of iron-peak elements by the circumstellar dust (Bond 1991; Lambert 1991; Van Winckel, Mathis, & Waelkens 1992). Van Winckel, Waelkens, & Waters (1995) found that many of these high-latitude stars are binaries, and they concluded that these more likely represent a particular stage of binary evolution rather than being typical post-AGB stars. (See also Van Winckel 1999 for a good summary).

Recently a subgroup of post-AGB candidates emerged with the discovery of a 21 μm emission feature in their mid-infrared spectra (Kwok, Volk, & Hrivnak 1989; Kwok, Hrivnak, & Geballe 1995; Omont et al. 1995; Kwok, Volk, & Hrivnak 1999). These studies showed that the 21 μm emission feature was not found either in PNs or in AGB stars, suggesting that it is only in the dust envelopes of transition objects (PPNs), under special physical conditions. Although the nature of the 21 μm emission feature is not known, a good correlation exits between the presence of carbon molecules such as C_2 and C_3 in the optical and the presence of the 21 μm feature (Hrivnak 1995; Bakker et al. 1996, 1997), which indicates that this feature originates in a carbon-rich dust envelope. Thus the presence of a 21 μm feature may be direct evidence of a carbon-rich dust envelope and hence a carbon-rich nature of the photosphere.

Elemental abundance analyses have recently been carried out for several 21 μm PPNs: IRAS 07134+1005 (HD 56126: Parthasarathy, García-Lario, & Pottasch

[1] Department of Physics and Astronomy, Valparaiso University, Valparaiso, IN 46383; ereddy@kepler.valpo.edu, bruce.hrivnak@valpo.edu.
[2] Visiting Astronomer, McDonald Observatory, operated by the University of Texas.
[3] Department of Astronomy and McDonald Observatory, University of Texas, Austin, TX 78712.
[4] TNO-FEL, Electro Optics Group, P.O. Box 96864, 2509 JG, The Hague, The Netherlands; e.j.bakker@fel.tno.nl.

TABLE 1

SOME OBSERVATIONAL PROPERTIES[a]

Parameter	Z02229+6208	07430+1115
V	12.1	12.6
$B-V$	2.8	1.9
l (deg)	133.7	208.9
b (deg)	+1.5	+17.1
Spectral type	G8–K0 0–Ia:	G5 0–Ia:
Infrared excess	Yes	Yes
21 μm emission	Yes	No

[a] Hrivnak & Kwok 1999.

1992; Klochkova 1995), IRAS 22272+5435 (HD 235858: Začs, Klochkova, & Panchuk 1995), IRAS 19500−1709 (HD 187885: Van Winckel, Waelkens, & Waters 1996), IRAS 05341+0852 (Reddy et al. 1997), and IRAS 22223+4727 and IRAS 04296+3429 (Decin et al. 1998). These indeed show large C/O ratios and *s*-process elemental enhancements, consistent with AGB nucleosynthesis, shell flashes, and dredge-up. Although these stars seem to represent clearly the post-AGB phase of evolution and the expected products of nucleosynthesis on the AGB phase, they also pose new questions. The *s*-process elemental distribution, represented by the ratio of heavy-to-light elements, [*hs*/*ls*], is found to be lower than expected (Decin et al. 1998). The finding of a high Li abundance in a few of these carbon-rich PPNs (Začs et al. 1995; Reddy et al. 1997) is surprising. Since Li is very fragile (easily destroyed at few times 10^6 K), its abundance is expected to be very low (Brown et al. 1989) owing to depletion in the pre–main-sequence and main-sequence phases and by dilution on the RGB and AGB phases where the stars develop deep convective envelope. The chemical composition analysis of more of this class of objects may serve to constrain the theoretical models and hence may lead to a better understanding of the role of thermal pulses, nucleosynthesis, mixing mechanisms, and the transition process of oxygen-rich to carbon-rich stars during the AGB phase of evolution.

In this paper we present detailed chemical composition analyses of two new PPNs, IRAS Z02229+6208 and IRAS 07430+1115. Both objects were initially chosen as PPN candidates based on their mid-infrared *IRAS* colors. Ground-based follow-up revealed them each to have a double-peaked spectral energy distribution, spectral type of G supergiants, and C_2 and C_3 absorption features. PAH features were also seen in both, with IRAS Z02229+6208 also possessing the 21 μm emission feature (Hrivnak & Kwok 1999). In Table 1 we summarize some of their observational properties. (Note that the letter "Z" in the name of IRAS Z02229+6208 indicates that this source is listed in the *IRAS* Faint Source Reject File but not in the *IRAS* Point Source Catalog or Faint Source Catalog; for details see, Hrivnak & Kwok 1999).

2. OBSERVATIONS

Spectra were obtained on 1996 December 19–23, with the McDonald Observatory 2.7 m telescope, using the cross-dispersed coudé echelle spectrograph (Tull et al. 1995) and a CCD of 2048 × 2048 pixels. Thirty-six spectral orders were recorded, providing spectral coverage from 5200 to 9800 Å with gaps between the orders. We obtained three or four 30 minute exposures for each of two settings, to improve the S/N ratio and also to correct better for cosmic ray hits. By combining the spectra, we achieved an average S/N ≈ 100 for IRAS Z02229+6208 and S/N ≈ 70 for IRAS 07430+1115. The spectral resolution is $R(\lambda/\Delta\lambda) \approx 55{,}000$, as measured from the Th-Ar arc spectral lines.

The observed spectra were reduced using the standard NOAO IRAF package. The spectra were bias subtracted, flat-field corrected to remove pixel-to-pixel variations, and converted to one-dimensional spectra. The spectra were wavelength calibrated using Th-Ar arc spectra obtained immediately following each observation. We also obtained spectra of several hot, rapidly rotating stars, which were used to identify the telluric absorption lines. The wavelength-calibrated spectra were normalized to the continuum, and the equivalent widths of the absorption lines were measured using the routines available in the SPLOT package of IRAF. The equivalent widths were measured by Gaussian fitting to the observed profiles.

3. SPECTRAL ANALYSIS

3.1. *Spectral Description*

Both stars show numerous sharp absorption lines in their spectra, typical of cool evolved supergiants. A few selected regions of the spectra of both the stars are presented in Figure 1. Several important lines are indicated on the spectra. The Li I resonance lines at 6707 Å and Al I lines at 6696 and 6698 Å have been identified in both of the spectra, as well as strong lines of the *s*-process elements Y II, La II, and Nd II (see Fig. 1). No atomic emission lines are seen. Both IRAS Z02229+6208 and IRAS 07430+1115 show circumstellar absorption lines of C_2 Phillips and CN Red system bands in their spectra. A complex series of Na I D lines and a series of K I lines are seen in the spectra of both stars. These will be discussed later.

3.2. *Radial Velocities*

A summary of the radial velocity measurements for both stars is presented in Table 2. We have chosen good lines for measuring the radial velocities of these stars, avoiding all lines that are very strong or asymmetric. To investigate radial velocity trends with the lower excitation potential (LEP) of an element, we have listed in Table 2 the average LEP ($\overline{\text{LEP}}$) and the average heliocentric radial velocity (V_r) for each element, along with the number of lines (n) used. The results do not show any obvious correlation between LEP and V_r except for the LEP = 0 lines, which are discussed below.

The lines of Na I (5890, 5896 Å), K I (7699 Å), and Li I (6707 Å) are shifted redward (∼0.2 Å) relative to lines of other atoms (Table 2). The average V_r of these zero LEP lines of Li I, Na I, and K I show radial shifts of $\sim +10$ km s^{-1} as compared to those of higher LEP lines. These are all resonance lines of neutral alkalis, so they all should be formed under similar conditions. It may be that these lines are formed in a distinct region with its own particular velocity. Monitoring of these stars for pulsations may help one to understand the displacement of these zero LEP lines. Recently, Gonzalez, Lambert, & Giridhar (1997) noticed a slight asymmetry in the profiles of Li, Na, and K in the high-resolution spectra of CE Vir, which might be due to the same physical mechanism.

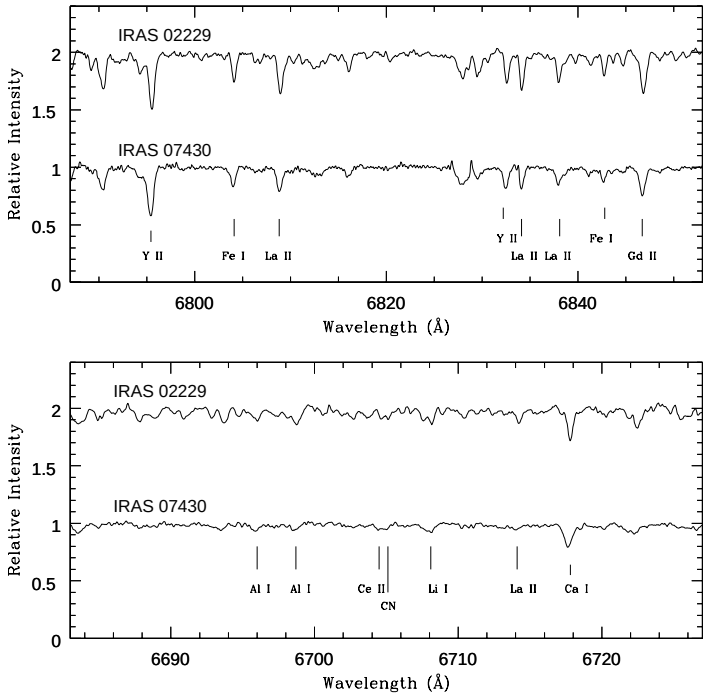

FIG. 1.—Sample spectra of IRAS Z02229 + 6208 and IRAS 07430 + 1115 showing the presence of Li, Al, and *s*-process elements

The radial velocity results for the $C_2(2,0)$, $C_2(3,0)$, and CN(1,0) molecular lines are also presented in the Table 2. These show a shift of ~ -12 km s^{-1} with respect to the atomic lines. The molecular spectra are discussed in detail in § 3.7.

3.3. *Line Selection and Atomic Data*

Identification of atomic lines has been made using the solar spectrum (Moore, Minnaert, & Houtgast 1966), supplemented with the line compilation by R. E. Luck (1993, private communication). For molecular C_2, C_3, and CN line identification, we used the lines listed by Bakker (1995). For the abundance analysis, we excluded all lines that are stronger than 200 mÅ, in order to minimize the effects due to uncertainties in the microturbulence value (ξ_t), damping parameter, and non-LTE effects. For the final abundance analyses, we tried to include as many lines as possible that were common to both PPNs. In some cases we were not able to do this owing to line asymmetries (we used only good lines), differences in line strengths due to the temperature difference between the two stars, and the lower signal-to-noise ratio in IRAS 07430 + 1115.

The oscillator strengths (log *gf*-values) for most of the lines were taken from Thévenin (1989, 1990), who derived *gf*-values by inverting the solar spectrum. For C I and N I, we used the theoretical *gf*-values calculated by Hibbert et al. (1991, 1993) and by Biémont et al. (1993). For additional lines (S I, Si I, and Mg I) not found in these papers, we used

TABLE 2

RADIAL VELOCITIES MEASURED FOR INDIVIDUAL SPECIES

	Z02229 + 6208			07430 + 1115		
SPECIES	*n*	$\overline{\text{LEP}}$(eV)	V_r(km s^{-1})	*n*	$\overline{\text{LEP}}$(eV)	V_r(km s^{-1})
C I	9	8.67	18±1	8	8.64	34±2
O I	3	9.14	17±1	3	9.14	34±1
Ca I	7	2.52	18±1	6	2.52	35±1
Fe I	16	3.20	18±1	20	3.25	34±2
Fe II	6	3.48	17±2	4	3.68	34±1
Ni I	7	3.35	19±2	6	3.60	35±2
Ce II	4	1.18	19±2	4	1.18	35±1
Nd II	9	1.10	20±2	8	1.10	36±3
CN (phot).....	2	...	14±2	...	...	...
Li I	1	0.0	26±1	1	0.0	50±2
Na I	2	0.0	30±2	2	0.0	46±3
K I.....	1	0.0	24±1	1	0.0	46±3
C_2 (2,0).....	23	...	6±1	15	...	22±1
C_2 (3,0).....	12	...	6±1	13	...	24±1
CN (1,0).....	7	...	8±1	6	...	24±1

NOTE.—The number of lines used in the velocity determination is indicated by *n*.

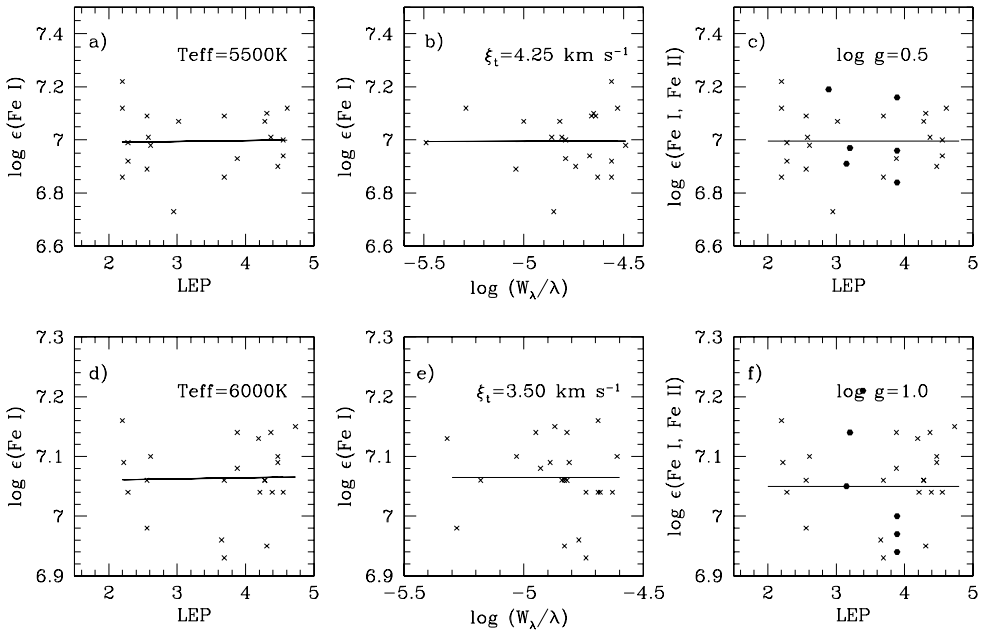

FIG. 2.—Spectroscopic determination of atmospheric parameters $T_{\rm eff}$, ξ_t, and log g using Fe I (*crosses*) and Fe II (*filled circles*) lines for both IRAS Z02229+6208 (*top panel*) and IRAS 07430+1115 (*bottom panel*) is shown.

gf-values from the line compilation of R. E. Luck (1993, private communication). For Al I *gf*-values, there exits a large discrepancy between the values of Thévenin (1989, 1990) and R. E. Luck (1993, private communicatin), and we adopted the values of Luck. (See § 3.6 for details.) For Fe I and Fe II lines, we used *gf*-values recently compiled by Lambert et al. (1996) and Giridhar & Arellano Ferro (1995), respectively.

3.4. *Atmospheric Parameters*

The atmospheric parameters of effective temperature ($T_{\rm eff}$) and surface gravity (log g) were initially estimated from the assigned spectral and luminosity classes. Hrivnak & Kwok (1999) classified IRAS Z02229+6208 and IRAS 07430+1115 as G8–K0 0–Ia: and G5 0–Ia:, respectively, based on their low-resolution optical spectra. The spectral type–$T_{\rm eff}$ calibration (Böhm-Vitense 1972) yields $T_{\rm eff}$ = 4430 K for IRAS Z02229+6208 and $T_{\rm eff}$ = 4850 K for IRAS 07430+1115.

Using the $T_{\rm eff}$ values determined above and log g = 1.0 (typical for a supergiant) as initial values, we derived the physical parameters spectroscopically by analyzing neutral (Fe I) and ionized (Fe II) lines of iron. We have chosen many Fe I and Fe II lines for the analysis.

The $T_{\rm eff}$ was determined by the method of excitation balance, constraining the Fe I abundance to be independent of the LEP of the individual lines. In deriving $T_{\rm eff}$, only weak Fe I (equivalent width [W_λ] ≤ 130 mÅ) lines have been used, to reduce the uncertainty due to microturbulence. In this way, we derived T = 5500 K for IRAS Z02229+6208 and 6000 K for IRAS 07430+1115. The microturbulent velocity (ξ_t) was determined by analyzing the reduced equivalent widths (W_λ/λ) of Fe I and Nd II lines. We adopted the value of ξ_t, which showed no correlation between the derived abundances and W_λ/λ. The log g was determined using the ionization equilibrium of Fe I and Fe II lines. The determination of $T_{\rm eff}$, log g, and ξ_t using Fe I and Fe II lines is illustrated in Figure 2. From this analysis, we found T = 5500 K, log g = 0.5, and ξ_t = 4.25 km s^{-1} for IRAS Z02229+6208, and T = 6000 K, log g = 1.0, and ξ_t = 3.50 km s^{-1} for IRAS 07430+1115. These results are listed in Table 3.

The non-LTE effects on the Fe I and Fe II lines in the spectra of the cool supergiant Arcturus have been discussed by Takeda (1991). The study of the non-LTE corrections versus W_λ and LEP indicates that for lines of $W_\lambda \leq$ 130 mÅ and LEP ≥ 3.5 eV, the non-LTE corrections are of minor important (Δ log $\epsilon \leq$ 0.1). Since most of the Fe I and Fe II lines used in this study have $W_\lambda \leq$ 130 mÅ, we do not expect significant non-LTE effects in our parameter determinations and subsequent abundance analysis.

We note that the values of $T_{\rm eff}$ derived in this study are ~1000 K higher than those estimated from their spectral classification. A similarly large temperature difference between the high-resolution analysis and the low-resolution spectral classification has also been observed by Decin et al. (1998) for similar carbon-rich PPNs. Spectroscopic indicators such as CH and CN bands and *s*-process elements may

TABLE 3

ATMOSPHERIC PARAMETERS DETERMINED FROM SPECTROSCOPIC ANALYSIS

Object	$T_{\rm eff}$(K)	log g	ξ_t(km s^{-1})	[M/H]	V_r(km s^{-1})
Z02229+6208.....	5500	0.5	4.25	−0.5	18±1
07430+1115	6000	1.0	3.50	−0.5	35±1

be affected by the enhancement of C, N, and *s*-process elements, which we will discuss later. Thus we suspect that these features may make carbon-rich and *s*-process–enriched post-AGB stars appear cooler in their low-resolution spectra.

The uncertainties in $T_{\rm eff}$, log g, and ξ_t have been estimated from the sensitivity of the abundance versus LEP correlation to changes in $T_{\rm eff}$ and log g and the abundance versus W_λ/λ to changes in ξ_t. After several iterations, we estimated the uncertainties in $T_{\rm eff}$ to be ± 250 K, in log g to be ± 0.25, and in ξ_t to be ± 0.5 km s^{-1}.

3.5. *Abundances*

3.5.1. *Fine Analysis*

The abundances are derived mostly by the fine analysis method, using the modified code MOOG, originally developed by Sneden (1973). In this method, for a given LTE model atmosphere, strength of the line, and relevant atomic data, MOOG adjusts the abundances such that the computed equivalent width matches with that of each individual observed spectral line. In this analysis we used LTE model atmosphere grids computed by Kurucz (1993).

Using this analysis, the average iron abundances were derived: log ϵ(Fe I) = 7.0 for IRAS Z02229+6208 and log ϵ(Fe I) = 7.1 for IRAS 07430+1115. These values are based on 22 Fe I lines for each star. The abundance results derived from individual lines of Fe I and Fe II, as well as for all of the individual lines of other atomic species, are listed in Table 10, along with their LEP values and log *gf*-values.

Summaries of the elemental abundances determined for both stars, based on the atmospheric parameters determined above and with a metallicity of [M/H] = −0.5, are listed as Model 1 in Tables 4 and 5. In these two tables, *n* represents the total number of lines used in the determination of each elemental abundance, log ϵ(X) is the standard notation for representing the elemental abundance and is defined as log [N(X)/N(H)]+12, and σ is the standard deviation (representing the line-to-line scatter in the abundance determinations of each element). The usual notation [X/H] is the logarithmic ratio with respect to hydrogen, relative to the solar value, and [X/Fe] = [X/H] − [Fe/H] denotes the logarithmic elemental abundance relative to the iron abundance (Fe I) in the program stars.

Of the CNO trio, we could determine the abundances of only C and N. We could not derive the oxygen abundance from O I because the O I triplet region at 6156 Å was missed in the gaps between the spectral orders. Unfortunately, the forbidden [O I] lines at 6300 and 6362 Å were contaminated by noise and atmospheric emission lines, rendering them useless for the abundance determination. We were left with the strong O I triplet lines at 7771 Å, which are well known for their non-LTE effects, and hence these lines were not used in our abundance analysis.

We derived the C and N abundances from many well-defined atomic, neutral carbon and nitrogen lines in the red part of the spectra. In order to determine accurate abundances for C and N, we searched the entire spectra to measure as many good lines as possible. This resulted in identifying as many as 14 C I lines, including the forbidden

TABLE 4

ELEMENTAL ABUNDANCE ANALYSES OF IRAS Z02229+6208

		MODEL 1 (5500 K)[a]—Adopted				MODEL 2 (5000 K)[b]			
SPECIES	*n*	log (X)	σ	[X/H]	[X/Fe]	log ϵ(X)	σ	[X/H]	[X/Fe]
Li I	1	(2.3)	...	...	...	(1.7)	...	...	...
C I	10	8.84	0.16	0.29	0.78	9.43	0.26	0.87	1.98
N I	5	8.67	0.01	0.70	1.19	9.51	0.06	1.46	2.57
Mg I	1	7.21	...	−0.37	0.14	6.80	...	−0.78	0.33
Al I	1	6.19	...	−0.28	0.21	5.85	...	−0.62	0.49
Si I	3	7.47	0.09	−0.08	0.41	7.17	0.05	−0.38	0.73
S I	2	7.07	0.03	−0.14	0.35	7.58	0.06	0.37	1.48
Ca I	8	6.04	0.14	−0.32	0.17	5.56	0.13	−0.72	0.39
Sc II	2	2.60	0.13	−0.57	−0.04	2.68	0.14	−0.42	0.69
Ti II	1	4.47	...	−0.55	−0.02	4.60	...	−0.39	0.72
Cr I	1	5.39	...	−0.28	0.21	4.86	...	−0.75	0.36
Cr II	2	5.39	0.09	−0.28	0.21	5.65	0.10	−0.02	1.09
Fe I	22	7.01	0.13	−0.49	0.00	6.44	0.16	−1.11	0.0
Fe II	6	7.09	0.14	−0.41	0.08	7.35	0.14	−0.17	0.94
Ni I	15	5.82	0.13	−0.43	0.06	5.25	0.21	−1.00	0.11
Y I	2	3.50	0.13	1.26	1.75	2.71	0.11	0 .47	1.57
Y II	2	3.86	0.12	1.62	2.11	3.91	0.16	1.67	2.78
Zr II	2	4.33	0.11	1.73	2.22	4.48	0.11	1.88	2.99
La II	2	1.94	0.01	0.72	1.21	2.07	0.05	0.85	1.96
Ce II	4	2.09	0.04	0.54	1.03	2.08	0.04	0.52	1.63
Pr II	3	1.79	0.08	1.08	1.57	1.71	0.06	1.00	2.11
Nd II	9	2.36	0.14	0.86	1.35	2.33	0.13	0.83	1.94
Sm II	1	1.40	...	0.39	0.88	1.41	...	0.41	1.52
Eu II	2	0.80	0.06	0.29	0.78	0.84	0.07	0.33	1.44
Gd II	1	1.37	...	0.25	0.74	1.40	...	0.28	1.39

NOTE.—The values in parentheses are derived from spectrum synthesis.

[a] Model 1: $T_{\rm eff}$ = 5500 K, log g = 0.5, ξ_t = 4.25 km s^{-1}, and [M/H] = −0.5.

[b] Model 2: $T_{\rm eff}$ = 5000 K, log g = 1.0, ξ_t = 4.25 km s^{-1}, and [M/H] = −0.5.

TABLE 5

ELEMENTAL ABUNDANCE ANALYSIS OF IRAS 07430+1115

		MODEL 1 (6000 K)[a]—Adopted				MODEL 2 (5500 K)[b]			
SPECIES	n	log ϵ(X)	σ	[X/H]	[X/Fe]	log ϵ(X)	σ	[X/H]	[X/Fe]
Li I	1	(2.4)	...	...	...	(1.9)	...	...	...
C I	11	8.76	0.13	0.21	0.63	9.05	0.20	1.30	2.05
N I	4	7.97	0.06	0.00	0.42	8.60	0.09	0.55	1.30
Mg I	1	7.19	...	−0.39	0.03	7.03	...	−0.55	0.20
Al I	1	5.96	...	−0.51	−0.09	5.84	...	−0.63	0.12
Si I	3	7.29	0.04	−0.26	0.16	7.18	0.08	−0.37	0.38
S I	2	6.98	0.02	−0.23	0.19	7.25	0.04	0.04	0.79
Ca I	5	6.02	0.08	−0.34	0.11	5.84	0.10	−0.52	0.23
Sc II	2	2.64	0.06	−0.46	−0.04	2.50	0.08	−0.60	0.15
Cr I	1	5.26	...	−0.41	0.01	4.97	...	−0.70	0.05
Cr II	1	5.26	...	−0.41	0.01	5.32	...	−0.35	0.40
Fe I	22	7.08	0.10	−0.42	0.00	6.77	0.13	−0.75	0.0
Fe II	6	7.00	0.14	−0.50	−0.08	7.03	0.14	−0.49	0.26
Ni I	11	5.89	0.06	−0.36	0.06	5.54	0.10	−0.71	0.04
Y II	2	3.72	0.25	1.48	1.90	3.57	0.023	1.33	2.08
Zr II	2	4.45	0.08	1.85	2.27	4.37	0.08	1.77	2.52
La II	2	2.45	0.06	1.23	1.65	2.31	0.07	1.09	1.84
Ce II	4	2.45	0.12	0.90	1.32	2.26	0.03	0.71	1.46
Pr II	1	2.54	...	1.83	2.25	2.26	...	1.55	2.30
Nd II	7	2.74	0.16	1.24	1.67	2.48	0.15	0.98	1.73
Sm II	1	1.65	...	0.64	1.06	1.44	...	0.44	1.19
Eu II	1	0.47	...	−0.04	0.38	0.30	...	−0.21	0.30
Gd II	1	1.40	...	0.28	0.70	1.25	...	0.13	0.90

NOTE.—The values in parentheses are derived from spectrum synthesis.

[a] Model 1: $T_{\rm eff}$ = 6000 K, log g = 1.0, ξ_t = 3.50 km s^{-1}, and [M/H] = −0.5.

[b] Model 2: $T_{\rm eff}$ = 5500 K, log g = 1.0, ξ_t = 3.50 km s^{-1}, and [M/H] = −0.5.

line at 8727.13 Å, and six N I lines. However the final carbon abundances, log ϵ(C) = 8.8 for IRAS Z02229+6208, and log ϵ(C) = 8.8 for IRAS 07430+1115, are based on only 10 and 11 lines, respectively. The abundance of nitrogen comes from five N I lines for IRAS Z02229+6208 [log ϵ(N) = 8.7] and four N I lines for IRAS 07430+1115 [log ϵ(N) = 8.0]. A few C I and N I lines were omitted owing to their asymmetric profiles. Studies of non-LTE effects on the C I and N I lines (Luck & Lambert 1985; Venn 1995) indicate that the non-LTE effects on the abundances of lines weaker than 100 mÅ and for the stars of $T_{\rm eff} \leq$ 6500 K are not important. We therefore applied no corrections, since most of the C and N lines we analyzed are weaker than W_λ = 100 mÅ and since no systematic difference in abundances is seen between the stronger and weaker lines.

We determined the abundances of the α-process elements Mg, Si, S, Ca, and Ti, and these are listed in Tables 4 and 5. Except for the abundance of Ca, the rest of the α-process elemental abundances are based on only a few lines. The abundance of Ca is based on five to eight Ca I lines of moderate strength and shows a deficiency of [Ca/H] = −0.3 for both stars. The abundances of Mg, Si, and S are found to be slightly overabundant in IRAS Z02229+6208 with respect to Fe. Also note that the uncertainties may be large, since many of these abundances are based on very few lines. The average abundance of the α-process elements is found to be normal relative to Fe ([α-process/Fe] = 0.1–0.2). The abundance of the odd-Z element Al was determined using only a single line of Al I at 6696.03 Å.

The abundances of iron-peak elements (Sc, Cr, Fe, and Ni) are found to be deficient ([Fe/H] = −0.4 to −0.5) in both stars, relative to their corresponding solar values. The abundance of Ni ([Ni/Fe] = 0.1) is derived from many good lines of weak and moderate strength, while the abundances of Sc and Cr are based on only a few lines.

In both of the spectra we could identify many ionized lines of heavy elements: Y, Zr, La, Ce, Pr, Nd, Sm, Eu, and Gd. Unfortunately we were not able to use all of these lines, since most of them are too strong (>200 mÅ) to be used in the abundances analysis and a few good ones lack atomic data, especially the lines occurring in the red part of the spectra. A few very strong Ba lines are seen in the spectra, but they are much too strong to use for abundance determinations. The average abundances for the elements Ce and Nd were derived from four or more lines, and these may best represent the s-process abundances for the stars. The rest of the abundances are mostly based on only one or two lines. We could positively identify two Y I lines at 6687.57 Å (W_λ = 40 mÅ) and 6793.63 Å (W_λ = 36 mÅ) in the spectrum of IRAS Z02229+6208 but not in IRAS 07430+1115; this may be due to the lower $T_{\rm eff}$ of IRAS Z02229+6208. The average Y I abundance [log ϵ(Y I) = 3.5] is found to be somewhat less than the Y II abundance [log ϵ(Y II) = 3.9], which may be due to the large difference in the strengths of the Y I and Y II lines. In fact, the derived abundances for heavy elements based on stronger lines are found to be highly sensitive to microturbulence, as discussed later in § 3.6. In spite of the large uncertainties (±0.2 to ±0.3) in the heavy element abundances derived by using stronger lines, the average s-process abundances based on elements Y, Zr, La, Ce, Pr, Nd, Sm, and Gd are clearly much larger than their corresponding solar values: [s-process/Fe] = 1.4 for IRAS Z02229+6208 and [s-process/Fe] = 1.6 for IRAS 07430+1115. Since the Eu abundance is mostly con-

tributed by the *r*-process, it has been excluded from the average *s*-process abundance value.

We also investigated the results derived from cooler temperature models, since the low-resolution spectra indicated a lower temperature. For IRAS Z02229+6208, we lowered $T_{\rm eff}$ from 5500 to 5000 K and for IRAS 07430+1115, from 6000 to 5500 K. These results are also listed in Tables 4 and 5 as Model 2. The abundances derived from the cooler models also indicate that the stars are metal-poor, with a clear overabundance of C, N, and *s*-process elements. However, these models result in a large discrepancy in the abundances of iron derived from the Fe I and Fe II lines; also the correlations of LEP versus abundances of Fe I lines show positive values of slope, indicating higher $T_{\rm eff}$ models. Had we used models with still lower temperatures, as indicated by the low-resolution spectra, the discrepancies would be even larger. Therefore, for our final discussion, we adopted the abundances derived using Model 1.

3.5.2. Li *Abundance from Spectrum Synthesis*

The lithium abundance can be derived from the Li I doublet line at 6707 Å. However, this line is expected to be blended with both the CN Red system and *s*-process lines in the spectra of cool post-AGB stars such as IRAS Z02229+6208 and IRAS 07430+1115. Thus the measured strength, as represented by its equivalent width, may lead to an overestimate of the Li abundance. We therefore used the spectrum-synthesis method, which takes into account the possible contributions by other nearby features and hence yields a more reliable abundance.

This method requires a complete line list with good atomic data for all the lines. An initial line list in the vicinity of the Li doublet line was taken from Kurucz & Petrymann (1975). This line list was modified to accommodate reliable *gf*-values and molecular CN lines according to the list given by Cunha, Smith, & Lambert (1995). In this line list we included all the hyperfine structure components of the Li doublet as discussed by Andersen, Gustafsson, & Lambert (1984). Also, we incorporated the suspected Ce II line at 6707.74 Å (Lambert, Smith, & Heath 1993).

In Figure 3 we compare the theoretical spectra with the observed spectra in the wavelength range 6705–6710 Å. The theoretical spectra were computed using the MOOG computer code (Sneden 1973) for three Li abundance values. We obtained the best fits with the observed spectra for Li abundance values of log ϵ(Li) = 2.3 for IRAS Z02229+6208 and log ϵ(Li) = 2.4 for IRAS 07430+1115. The synthetic spectra were convolved with a Gaussian profile of FWHM $\approx$ 0.3 Å, which incorporated both the instrumental broadening and the macroturbulent velocity, $v_m \approx 6$ km s^{-1}. This value for v_m was estimated by fitting synthetic spectra to the observed spectra for a few weak Fe I lines for which the abundance was determined independently by fine analysis. In computing the synthetic spectra, we incorporated the elemental abundances given in Tables 4 and 5.

The Li line in the spectrum of IRAS 07430+1115 appears weak when compared with the relatively strong Li line in IRAS Z0229+6208 and does not have as high a signal-to-noise ratio. The relative weakness is not surprising, since the temperature of IRAS 07430+1115 is higher by 500 K. However, we believe that the Li feature is definitely present in IRAS 07430+1130. We note that the feature is seen in our two individual spectra taken at the two different settings.

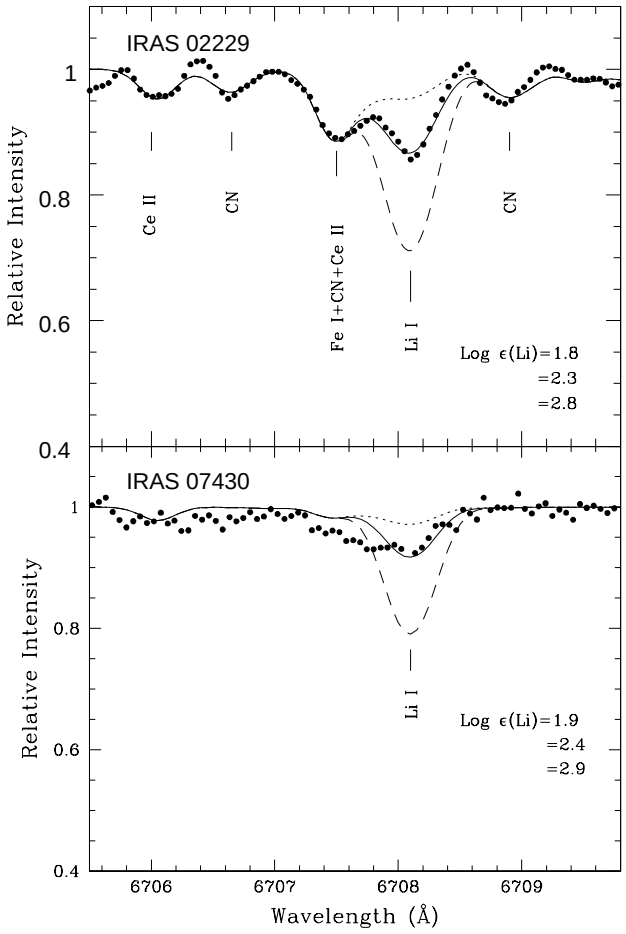

FIG. 3.—Synthetic spectrum around the Li I 6707 Å region is compared with the observed spectrum (*dots*) for both of the stars. Synthetic spectra are computed for three values of the Li abundance.

We have already noted in the discussion of radial velocities that the Li doublet is slightly shifted redward from its expected position. The positional matching of the synthetic Li profile with the observed one was achieved by simply adding the shift $\Delta\lambda = 0.2$ Å to the rest wavelengths of the Li lines. Another way to explain the shift in Li wavelength is to assume that the entire Li abundance is in the form of ^{6}Li rather than ^{7}Li. However, this seems unlikely based on other observations, which show an abundance ratio of ^{6}Li/^{7}Li = 0–0.5 (Andersen et al. 1984, and references therein).

We also note that the computed spectrum for IRAS 07430+1115 does not account for a small dip slightly shortward of the fitted Li line. This dip occurs at 6707.8 Å, which is the expected, unshifted Li position. Since the Li abundance has important implications, we investigated if this could possibly be the Li line. We fitted the observed spectrum (without adding 0.2 Å shift to the rest wavelength) and computed a Li abundance of log ϵ(Li) = 2.2; however, the theoretical spectrum then did not account for the line at 6708.05 Å. We conclude that the Li I doublet line is present and shifted, since this also is the case for similar lines of Na I and K I. Thus we discuss only the abundances derived from the shifted Li line, which are presented in Tables 4 and 5.

3.6. *Uncertainties*

To determine the uncertainties in our abundance values, we investigated the effects on the abundances due to the

estimated uncertainties in our adopted model parameters: $T_{\rm eff} = \pm 250$ K, $\log g = \pm 0.25$, and $\xi_t = \pm 0.5$ km s^{-1}. The corresponding abundance shifts for the uncertainties in the atmospheric parameters are tabulated in Table 6. They suggest that the abundances derived from lines of $W_\lambda \leq 125$ mÅ are not very sensitive to ξ_t. However, the uncertainty in ξ_t introduces an uncertainty of 0.1–0.2 dex in the abundances derived from the stronger lines. At the temperature of these stars, the derived abundances are very sensitive to changes in $T_{\rm eff}$, which introduces an uncertainty in the abundances [$\log \epsilon$(X)] of $\sim$0.1–0.3. The abundance of Li is found to be especially sensitive to $T_{\rm eff}$ and almost insensitive to the uncertainties in both $\log g$ and ξ_t. The uncertainties in $\log g$ are small and mainly affect the abundances of ionized species.

Other important sources of uncertainties in the derived abundances may be due to uncertainties in the adopted *gf*-values and to some extent to the measured equivalent widths of the lines. The differences between *gf*-values of Thévenin and another widely used source, Führ, Martin, & Wiese (1988), may alone contribute additional uncertainties of around 0.1–0.2 dex in the abundances (Thévenin 1989, 1990). We also investigated these possible uncertainties by computing abundances using *gf*-values from other sources. The Fe II *gf*-values derived from experiments and recently compiled by Giridhar & Arellano Ferro (1995) are systematically higher than the *gf*-values of Thévenin. The mean Fe II abundance [$\log \epsilon$(Fe II)] computed using the values of Thévenin is almost 0.2 dex higher than the abundance we derived using the values of Giridhar & Arellano Ferro. However the discrepancy between the *gf*-values for Fe I lines of Thévenin and the recently adopted *gf*-values of Lambert et al. (1996) is negligibly small; the average computed Fe I abundance using the common lines in both the sources differs by less than 0.05. We noticed a large difference in the Al I *gf*-values of Thévenin and the *gf*-values listed in the R. E. Luck (1993, private communication) compilation. Using the Thévenin solar *gf*-value of the Al I line at 6696.03 Å leads to an abundance that is 0.35 larger than the value we determined using the *gf*-value of Luck. This emphasizes the need for more accurate *gf*-values to determine accurate stellar abundances.

The uncertainties in the measured W_λ, due to incorrect placement of the continuum and to noise, may amount to 5%–15%, which yields additional uncertainties in the abundances in the range of 0.05 to 0.1 dex. The line-to-line scatter in the abundances (see Tables 4 and 5), as represented by σ, is mainly contributed by uncertainties in the *gf* values and the measured W_λ. Note that the main conclusions of our abundance studies are based on abundance ratios, which are much less affected by uncertainties in $T_{\rm eff}$, $\log g$, and ξ_t than are the absolute abundance values.

3.7. *Circumstellar Molecular Absorption Lines*

Both IRAS Z02229+6208 and IRAS 07430+1115 show circumstellar absorption lines in their spectra. Sample spectra showing circumstellar molecular C_2 Phillips (2,0) and CN Red system (2,0) bands, along with computed spectra, are shown in Figure 4. We also see photospheric CN absorption bands in IRAS Z02229+6208 (see Fig. 3), as found by Bakker et al. (1997) for several similar carbon-rich PPNs. These photospheric CN bands yield an average

TABLE 6

UNCERTAINTIES IN THE DERIVED ABUNDANCES

	Z02229+6208				07430+1115			
SPECIES (1)	$\overline{W_\lambda}$ (mÅ) (2)	$\Delta\xi_t$ ± 0.5 (km s^{-1}) (3)	$\Delta T_{\rm eff}$ ± 250 (K) (4)	$\Delta \log g$ ± 0.25 (5)	$\overline{W_\lambda}$ (mÅ) (6)	$\Delta\xi_t$ ± 0.5 (km s^{-1}) (7)	$\Delta T_{\rm eff}$ ± 250 (K) (8)	$\Delta \log g$ ± 0.25 (9)
Li I	65	0.01	0.30	0.01	40	0.01	0.25	0.01
C I	89	0.03	0.15	0.08	95	0.04	0.07	0.11
N I	68	0.03	0.30	0.12	49	0.02	0.22	0.17
Mg I	97	0.03	0.06	0.01	89	0.05	0.09	0.03
Al I	53	0.02	0.05	0.03	31	0.02	0.12	0.07
Si I	125	0.05	0.07	0.01	93	0.05	0.11	0.04
S I	54	0.02	0.14	0.06	77	0.05	0.05	0.10
Ca I	126	0.07	0.14	0.02	86	0.05	0.15	0.04
Sc II	173	0.08	0.07	0.08	125	0.09	0.11	0.15
Cr II	110	0.04	0.05	0.08	80	0.01	0.21	0.04
Fe I	123	0.07	0.21	0.02	93	0.07	0.17	0.04
Fe II	130	0.07	0.02	0.08	87	0.06	0.04	0.14
Ni I	100	0.03	0.20	0.02	81	0.05	0.20	0.04
Y II	140	0.05	0.13	0.08	150	0.15	0.12	0.15
Zr II	203	0.13	0.02	0.09	164	0.15	0.08	0.08
La II	180	0.13	0.07	0.08	170	0.22	0.12	0.12
Ce II	160	0.08	0.10	0.08	146	0.16	0.15	0.14
Pr II	187	0.10	0.15	0.08	190	0.26	0.21	0.11
Nd II	140	0.10	0.12	0.10	154	0.19	0.18	0.12
Sm II	130	0.05	0.09	0.08	75	0.04	0.15	0.14
Eu II	100	0.03	0.06	0.08	55	0.02	0.14	0.07
Gd II	60	0.01	0.08	0.08	35	0.01	0.12	0.14

NOTE.—The uncertainties in the derived abundances [$\Delta \log \epsilon$(X)] are due to uncertainties in the atmospheric parameters, as listed in the column readings. W_λ represents the average equivalent widths of the lines for each element.

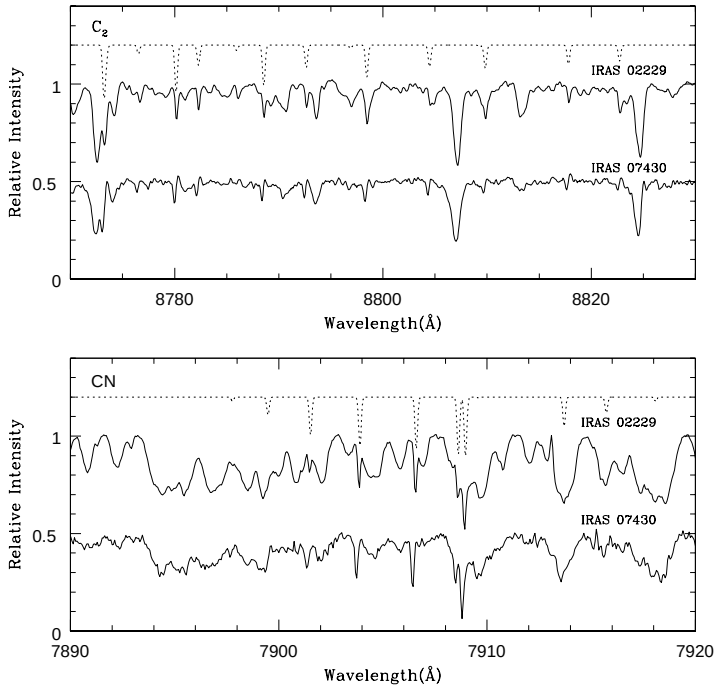

FIG. 4.—C_2 Phillips System (2–0) band (*upper panel*) and CN Red system band (*lower panel*) absorption features in IRAS Z02229+6208 and IRAS 07430+1115. Note that for IRAS 07430+1115, the C_2 lines have a P Cygni shape. In both of the panels, synthetic spectra are plotted, which were computed using $T_{rot} = 345$ K, log $N = 15.11$ cm^{-2}, $b = 0.51$ km s^{-1}, and $R = 55{,}000$.

radial velocity of $V_r = 14 \pm 2$ km s^{-1}, which is close to the radial velocity derived from photospheric atomic lines (Table 2).

From the molecular C_2 (3–0 and 2–0) lines we find radial velocities of $V_r = 6.0 \pm 1.0$ km s^{-1} and $V_r = 23.0 \pm 1.1$ km s^{-1}, and from the molecular CN lines (1–0) we find $V_r = 8 \pm 1$ km s^{-1} and $V_r = 24 \pm 1$ km s^{-1} for IRAS Z02229+6208 and IRAS 07430+1115, respectively (see Table 2). These molecular velocities are less than the photospheric values of 18 ± 1 km s^{-1}, and 35 ± 1 km s^{-1} for IRAS Z02229+6208 and IRAS 07430+1115, respectively, and are presumably formed in an expanding circumstellar envelope around each star. These molecular velocities can be compared with the photospheric values to derive expansion velocities of the envelopes, although, owing to possible pulsation of the photospheres, these can be uncertain by a few km s^{-1}. This matter is discussed more carefully in § 4.3.

Equivalent widths of the lines used in our rotational analysis were measured by making a Gaussian fit to the observed line profiles, using SPLOT in IRAF. Only those lines that had a unique identification and were not blended were used. While there are many molecular lines in the spectra, unfortunately there are not many that were well isolated and of sufficient quality to use in the analysis.

Column densities were computed using the optical-thin formula and by constructing a rotational diagram for both C_2 and CN. Adopting a Doppler parameter of $b = 0.51$ km s^{-1} (Bakker & Lambert 1998), we find that the optical-thin approximation breaks down for equivalent widths in excess of 80 mÅ. For IRAS Z02229+6208 there are only two lines that have an equivalent width in excess of 80 mÅ, while there are no lines for IRAS 07430+1115 in excess of 80 mÅ. Therefore, it seems appropriate to use the optical-thin formula in order to compute column densities. Required oscillator strengths for C_2 and CN were taken from Bakker et al. (1997). C_2 is a homonuclear molecule without any permanent dipole moment. Only even rotation levels ($J'' = 0, 2, 4, 6 \ldots$) exist, and the molecule has no infrared ro-vibrational spectrum. Stellar photons excite the molecule, but the molecule is not able to cool efficiently and the rotational temperature will be suprathermal ($T_{rot} \geq T_{kin}$). Therefore there is no unique rotational temperature for the C_2 molecule. In order to quantify the rotation temperature and to be able to compare it with C_2 in the line of sight to other stars, we determined an effective rotational temperature by fitting a first-order polynomial to the rotational diagram (effectively assuming that the molecule is in LTE). The fits yield the following for C_2: $T_{rot} = 354 \pm 53$ K and log $N = 15.30 \pm 0.10$ cm^{-2} for IRAS Z02229+6208, and $T_{rot} = 235 \pm 27$ K and log $N = 15.03 \pm 0.10$ cm^{-2} for IRAS 07430+1115, based on 34 and 24 lines, respectively. These rotational diagrams and the calculated fits are shown in Figure 5. CN is a heteronuclear molecule with a strong permanent dipole moment. All energy levels exist ($N'' = 0, 1, 2 \ldots$). The infrared and radio spectra of CN allow the molecule to cool below the kinetic temperature of the gas. The molecule will be subthermal ($T_{rot} \leq T_{kin}$). Only three lines are available for the CN molecule, and the rotational diagram does not very well constrain the rotational temperature and column density of CN in the line of sight to the two stars. Nevertheless, a fit to the rotational diagram of CN yields the following: $T_{rot} = 16 \pm 5$ K and log $N = 14.4 \pm 0.3$ cm^{-2} for IRAS Z02229+6208, and $T_{rot} = 9 \pm 5$ K, log $N = 14.3 \pm 0.3$ cm^{-2} for IRAS 07430+1115.

3.8. Na I D *Lines*, K I *Lines, and DIBs*

The complex structure of the Na I D_1 & D_2 lines in the spectra of IRAS Z02229+6208 and IRAS 07430+1115 are

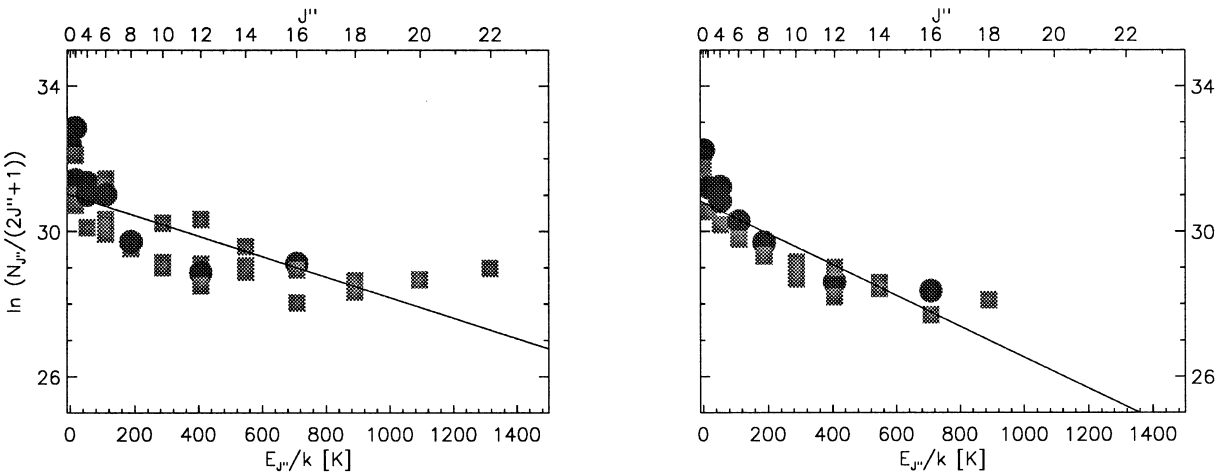

FIG. 5.—Rotational diagram for C_2 (2–0) (*circles*) and (3–0) (*squares*) bands toward IRAS Z02229+6208 (*left*) and IRAS 07430+1115 (*right*)

shown in Figure 6. We could identify at least six Na I components in the spectrum of IRAS Z02229+6208 and three components in the spectrum of IRAS 07430+1115. The detailed analysis of the Na I lines for both of the stars is given in Table 7. Since these two stars have strong infrared excesses and CO emissions arising from detached shells of cool dust and molecular gas (Hrivnak & Kwok 1999), they might be expected to show a circumstellar contribution to the Na I lines. By comparing the average measured radial velocities of atomic (Table 2) and molecular lines (Table 7), we found that components 1 and 2 appear to be of photospheric and circumstellar origin, respectively. Recently, Dinerstein, Sneden, & Uglum (1995) in the spectra of planetary nebulae, Bakker et al. (1996) in the spectrum of the PPN HD 56126, and Reddy & Hrivnak (1999) in the spectrum of the PPN candidate HD 179821, showed the presence of circumstellar Na I components.

Components 3, 4, 5, and 6 in the spectrum of IRAS Z02229+6208 and component 3 in the spectrum of IRAS 07430+1115 are presumably due to interstellar clouds in the line of sight. Using these radial velocities, we calculated the kinematic distances to the clouds based on a simple Galactic rotation model. This yields distances of 0.3, 1.0, 2.6, and 4 kpc for components 3, 4, 5, and 6, respectively, for IRAS Z02229+6208, and a distance of 0.3 kpc for component 3 of IRAS 07430+1115. In fact, IRAS Z02229+6208 is found to be in the direction of the W3 molecular cloud, and the radial velocity of component 5 ($V_{lsr} = -41$ km s^{-1}) is in good agreement with the radial velocity of the W3 cloud ($V_{lsr} = -43$ to -47 km s^{-1}) as measured from OH emission (Wilson, Johnston, & Mauersberger 1991). Since the W3 molecular cloud is determined to be at a distance of around 2.2 kpc (Wilson et al. 1991), this suggests that IRAS Z02229+6208 must be farther than the

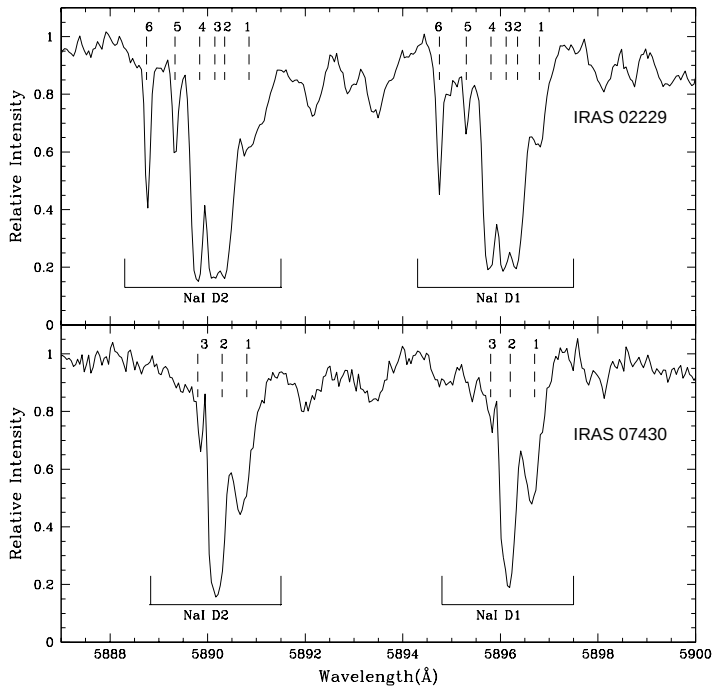

FIG. 6.—The Na I D_2 and D_1 absorption profiles of IRAS Z02229+6208 and IRAS 07430+1115 show six and three well-separated components, respectively. The corresponding line velocities are given in Table 7.

TABLE 7

ANALYSIS OF Na I AND K I LINES

	Z02229+6208				07430+1115			
	Na I D_2		Na I D_1		Na I D_2		Na I D_1	
COMPONENT	W_λ (mÅ)	V_r (km s^{-1})	W_λ (mÅ)	V_r (km s^{-1})	W_λ (mÅ)	V_r (km s^{-1})	W_λ (mÅ)	V_r (km s^{-1})
1	150	30	180	30	280	46	270	46
2	380	6	240	6	365	21	360	20
3	400	−4	250	−6	60	4	80	4
4	220	−21	180	−22	...	...	...	...
5	57	−45	55	−44	...	...	...	...
6	75	−73	75	−73	...	...	...	...
	K I λ7699		K I λ7665		K I λ7699		K I λ7665	
1	170	24	...[a]	...[a]	120	46	...[a]	...[a]
2	180	9	220	9	164	26	200	26
3	190	−7	...[b]	...[b]	...	...	...	...
4	30	−18	...[b]	...[b]	...	...	...	...

[a] Blended with telluric O_2 line at 7665.9 Å.
[b] Blended with telluric O_2 line at 7664.9 Å.

W3 cloud. In the case of IRAS 07430+1115, we identified only one interstellar component, which may be due to a very nearby cloud. This difference is understandable, since IRAS 07430+1115 lies above the Galactic plane with a latitude $b = 17^\circ.1$ while IRAS Z02229+6208 lies in the plane ($b = 1^\circ.5$), and its light is intercepted by many foreground interstellar clouds.

The structure of the K I lines in the spectra of IRAS Z02229+6208 and IRAS 07430+1115 is shown in Figure 7. For IRAS Z02229+6208 we can see four components of the profile at λ7699, while for IRAS 07430+1115 we can see two. The measured profiles of these lines are listed in Table 7. The velocities of these components show that components 1 and 2 are due to the photosphere and circumstellar envelope, respectively. Components 3 and 4 of IRAS Z02229+6208 may be due to interstellar clouds. The line at λ7665 is made complicated by the presence of two very strong telluric O_2 lines, as seen in the figure. For both stars, component 1 appears to be blended with the telluric O_2 line at 7665.9 Å. However, for both stars, component 2 is visible and of a velocity similar to that of component 2 of the profile at 7699 Å. Components 3 and 4 for IRAS Z02229+6208 appears to blended with telluric line at 7664.9 Å and to contribute to

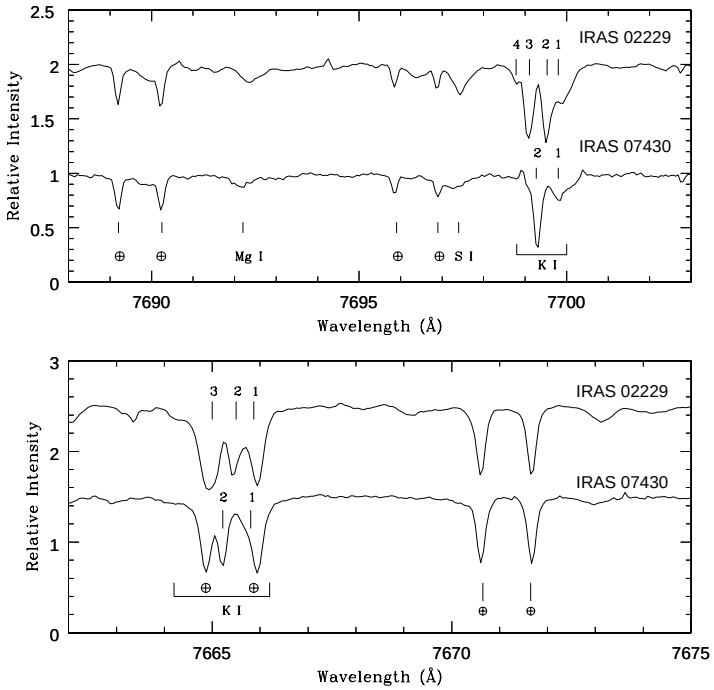

FIG. 7.—K I absorption profiles at 7699 Å (*top*) and 7665 Å (*bottom*). Components 1, 3, and 4 at 7665 Å are blended with telluric lines. The telluric O_2 (*Earth symbol*) lines are also marked and illustrate radial velocity shifts in the K I components between the two objects.

its having an unusually large relative equivalent width. These velocities are similar to those of the similar components seen in the Na I profiles (see Table 2).

K I and Na I lines due to fluorescent emission have previously been seen in emission in the circumstellar envelopes of supergiants (Mauron & Querci 1990) and giants (Plez & Lambert 1994).

We also investigated the presence of diffuse interstellar bands (DIBs) in the spectrum of these two objects. DIBs at 5780 and 6284 Å are seen in the spectrum of IRAS Z02229+6208, and perhaps at 5780 Å in the spectrum of IRAS 07430+1115. The measured velocity of the 5780 Å feature in IRAS Z02229+6208 is in good agreement with that of component 6 of Na I, suggesting that they both arise in the same interstellar cloud.

4. DISCUSSION

4.1. *General Abundance Patterns*

Summaries of our results on the chemical composition of IRAS Z02229+6208 and IRAS 07430+1115, based on the derived LTE model atmospheres, are listed as Model 1 in Tables 4 and 5. These are also presented visually in Figure 8. Inspection of the results in these tables and the abundance patterns in Figure 8 shows that these stars are slightly metal-poor and are overabundant in C, N, and *s*-process elements.

The enhancements in C and N are presumably the results of CN and 3α reactions and the mixing of these elements from the He-burning shell to the surface (third dredge-up) during the AGB phase. The overabundances of *s*-process elements result from neutron irradiation of the interior material and the deep convective mixing during the advanced stages of AGB evolution. The primary source of neutrons may be the activation of the $^{13}C(\alpha, n)^{16}O$ reaction as suggested by AGB models (Hollowell & Iben 1989; Busso et al. 1992). During the thermal pulses, a convective shell is formed between the base of the hydrogen-rich envelope and the helium-burning region. The large amount of helium in the convective shell coupled with the high temperatures (in excess of 150×10^6 K) at the base of the shell may allow (α,*n*) reactions to produce neutrons, which are then captured by iron seed nuclei to produce the observed *s*-process elements (Iben & Renzini 1982; Gallino et al. 1988). These temperatures are easily encountered in the intershell convective zone models for AGB stars (Iben 1981).

The ratio ([*hs*/*ls*]) of heavy (La, Ce, Pr, Nd) to light (Zr, Y) *s*-process elements is a good indicator of the mean neutron exposure rate τ_0 in the processed material (Luck & Bond 1991). This basically indicates to what extent the material in the convective layers was exposed to neutron flux. The higher the value of [*hs*/*ls*] (or τ_0), the higher the exposure. For IRAS Z02229+6208 and IRAS 07430+1115, the ratio [*hs*/*ls*] is found to be −0.7 and −0.4, respectively. By comparing these observed ratios with those of theoretical predictions of s-process elemental mixing on the AGB (Busso et al. 1995), we obtain τ_0 to be in the range 0.15–0.25 mbarn^{-1}.

We also determined the values of τ_0 by comparing the observed individual *s*-process abundances with Malaney's (1987) predicted *s*-process abundances for different models with an exponentially decaying neutron exposure. The observed *s*-process abundances were first corrected for the initial unexposed stellar material as explained by Smith et al. (1996). We fitted these observed abundances with each of the different τ_0 models, with a neutron density of $N_n = 10^8$ cm^{-3}. The best goodness of fit (minimum S^2) for each star was obtained with the model of $\tau_0 = 0.2$ mbarn^{-1}. We compare the observed *s*-process enhancements with the predicted values of the exponential neutron exposure models of Malaney (1987) in Figure 9. The basic fit is good and also shows that the odd-even (low-high) effect is observed in the abundances.

These values are similar to the τ_0 values recently obtained for other carbon-rich PPNs. In Table 8, we list for comparison the values of [Fe/H], [*hs*/*ls*], and τ_0 for

TABLE 8

RATIOS OF HEAVY TO LIGHT *s*-PROCESS ELEMENTS ([*hs*/*ls*]) AND MEAN NEUTRON EXPOSURE (τ_0) FOR CARBON-RICH PPNS

Object	[Fe/H]	[*hs*/*ls*]	τ_0 (mbarn^{-1})	References
IRAS Z02229+6208.....	−0.49	−0.7	~0.2	1
IRAS 04296+3429	−0.70	−0.3	~0.2	2
IRAS 05431+0852	−0.90	+0.5	~1.0	3
IRAS 07134+1005	−1.20	−0.1	~0.4	4
IRAS 07430+1115	−0.42	−0.4	~0.2	1
IRAS 22223+4327	−0.40	−0.6	~0.2	2
IRAS 22272+5435	−0.49	−0.0	~0.4	5

REFERENCES.—(1) This study; (2) Decin et al. 1998; (3) Reddy et al. 1997; (4) Hrivnak et al. 1999; (5) Začs et al. 1995.

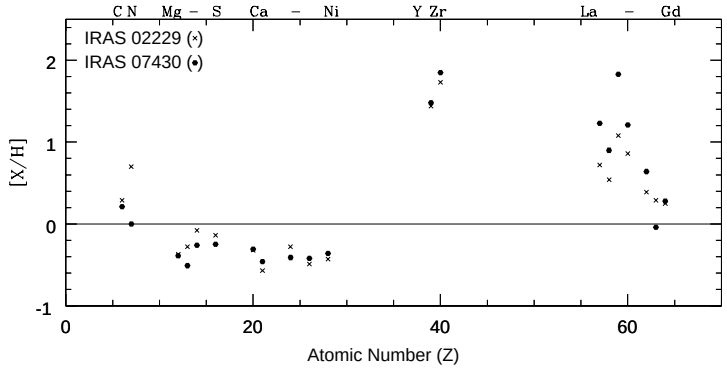

FIG. 8.—Elemental abundances relative to the solar value ([X/H]) vs. atomic number (Z) are shown for IRAS Z02229+6208 (*crosses*) and IRAS 07430+1115 (*hexagons*).

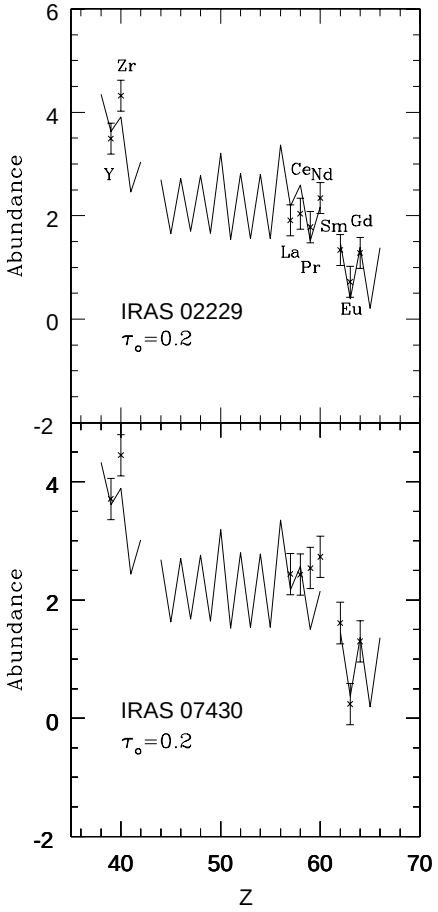

FIG. 9.—Comparison of the enhanced observed *s*-process elemental distribution with Malaney's (1987) theoretical distribution, for models of $\tau_0 = 0.2\,\mathrm{mbarn}^{-1}$ and $N_n = 10^8\,\mathrm{cm}^{-3}$.

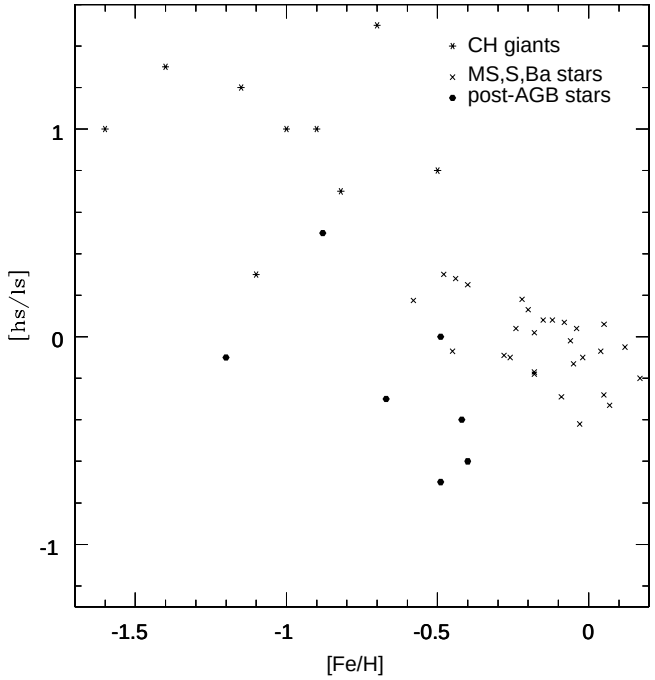

FIG. 10.—The values of [*hs*/ls] as a function of [Fe/H] for seven carbon-rich post-AGB stars are compared with metal-poor CH giants, MS, S, and Ba stars.

IRAS Z02229+6208 and IRAS 07430+1115 together with those of other known carbon-rich PPNs.

The [*hs*/*ls*] ratios of these carbon-rich post-AGB stars are distinctly lower than the values found for AGB stars, such as metal-poor CH giants (Kipper et al. 1996; Luck & Bond 1991), and MS, S, and Ba stars (Busso et al. 1995 and references therein). In Figure 10 we plot [*hs*/*ls*] versus [Fe/H] data for three groups of stars: (1) metal-poor CH giants; (2) MS, S, and Ba stars; and (3) carbon-rich post-AGB stars (PPNs). In the MS, S, and Ba star data, a general trend can be seen in the values of [*hs*/*ls*] with [Fe/H]. When these data are combined with those of the CH giants, this trend is even more pronounced. One can clearly see the expected anticorrelation between [*hs*/*ls*] and [Fe/H]. A decrease in metallicity from +0.2 (MS, S, and Ba) to −1.5 (metal-poor CH giants) is correlated with an increase in [*hs*/*ls*] from about −0.3 to 1.2. The expectation that [*hs*/*ls*] should show an inverse relation with metallicity is based on the fact that a low-metallicity environment in a AGB star favors synthesis of more heavier *s*-process elements and hence larger values of [*hs*/*ls*] for metal-poor stars.

In the case of PPNs, one can draw two tentative conclusions from Figure 10. The first is that the values of [*hs*/*ls*] for the set of carbon-rich post-AGB stars are less than the values for members of the other two groups at similar metallicity. The second is that the ratio [*hs*/*ls*] for PPNs also seems to show an anticorrelation with metallicity. However, the anticorrelation shows large scatter and is based on only a small number of data points. The scatter may be due to the fact that the abundance values were taken from different investigators, who derived these values from various quality spectra (both in S/N and resolution) using different methods, and by using slightly different sets of elements in deriving [*hs*/*ls*]. The observed lower value of [*hs*/*ls*] for the post-AGB stars indicates a less efficient *s*-process mechanism as compared to their counterparts on the AGB. To arrive at a more definite conclusion about the observed *s*-process distribution in carbon-rich post-AGB stars, it would be helpful to have a larger sample, with a wider range in metallicity. Such a study has the potential to help us understand the complexity involved in He-shell flashes and the third dredge-up during the AGB phase.

With the addition of these two stars, the number of PPNs that are found to display clear overabundances in C, N, and *s*-process elements rises to eight. In addition to the five others listed in Table 8 is IRAS 19500−1709 (HD 187885; Van Winckel et al. 1996). Interestingly, all of these stars except IRAS 07430+1115 (Hrivnak & Kwok 1999) have been shown to possess the 21 μm emission feature in their mid-infrared spectra. All of the 21 μm emission sources that have high-resolution spectroscopic studies (seven of 12) show from their abundance patterns that they are clearly post–third dredge-up, post-AGB/PPNs. It may be that IRAS 07430+1115 possesses a very weak 21 μm feature that will be detected with higher signal-to-noise ratio observations.

The α-process elements Mg, Si, Ca, and Ti are found to be normal relative to Fe. The abundance of Al is found to be low: [Al/Fe] = +0.06 and [Al/Fe] = −0.06 for IRAS Z02229+6208 and IRAS 07430+1115, respectively. Models of "hot bottom burning" (HBB) on the AGB indicate an enhancement of Al (Lattanzio et al. 1997) along with

Li. The high value of Li and normal Al abundance may suggest that these stars have not experienced a strong HBB.

4.2. Li *Abundance and Luminosity*

An important result of this study is the finding that these two PPNs are overabundant in Li [$\log \epsilon(\mathrm{Li}) = 2.3$ and 2.4 for IRAS Z02229+6208 and IRAS 07430+1115, respectively]. The value of $\log \epsilon(\mathrm{Li})$ for these stars is higher than that observed for typical red giants [$\log \epsilon(\mathrm{Li}) = -1$ to 1; Brown et al. 1989]. The obvious interpretation is that Li has been synthesized in these two stars. A high Li abundance has been reported previously in a few similar carbon-rich PPNs, IRAS 22272+5435 (Začs et al. 1995) and IRAS 05431+0852 (Reddy et al. 1997). Luck, Bond, & Lambert (1990) found a high Li abundance [$\log \epsilon(\mathrm{Li}) = 2.4$] in the F2 post-AGB supergiant HR 7671. HR 7671 is metal-poor ([Fe/H] $= -1.1$), shows significant *s*-process enhancement, but is slightly deficient in carbon.

The finding of large amounts of Li in many AGB stars in the Small Magellanic Cloud (SMC; Smith & Lambert 1989, 1990) led to the idea of Li being synthesized in evolved stars. It is believed to be produced by the ^{7}Be transport mechanism as first suggested by Cameron & Fowler (1971). Theoretical computations based on HBB models satisfactorily reproduced the large amounts of Li observed in the Li-rich stars of the SMC (Sackmann & Boothroyd 1992). These theoretical models suggest that HBB is only possible in very luminous ($M_{\mathrm{bol}} \approx -6$ to -7) and massive (4–7 $M_\odot$) AGB stars. The Li-rich stars found in SMC (Smith & Lambert 1989, 1990) are indeed luminous stars.

It is hard to compare the luminosities of individual post-AGB stars with these theoretical models since accurate distances are difficult to determine. But at least for IRAS Z02229+6208, the interstellar Na I components indicate that the star is at a distance of $d \geq 2.2$ kpc (see § 3.8). Assuming this distance, we can determine an approximate luminosity for the star based on its observed parameters (Table 1) and the total reddening (interstellar + circumstellar) of $\sim$2.1 mag. This value of the total reddening has been estimated from the difference between the observed $B-V$ and the expected value of $B-V$ for the atmospheric parameters derived in this analysis. This leads to a lower limit for the luminosity of $M_{\mathrm{bol}} \leq -6$ (which implies $M_{\mathrm{initial}} > 3\ M_\odot$). (Note that we get the same approximate value using the scaled flux determined by Hrivnak & Kwok 1999, when corrected for interstellar extinction.) Thus the overabundance of Li and its high luminosity may suggest that HBB existed in IRAS Z02229+6208 during its AGB phase of evolution.

Unfortunately we were not able to determine the oxygen abundance to quantify the C/O ratio for IRAS Z02229+6208 and IRAS 07430+1115. However, the detection of infrared PAH features at 3.3 and 11.3 μm, and the presence of strong molecular C_2 and C_3 lines in the optical spectrum (Hrivnak & Kwok 1999), suggest these stars are carbon-rich rather than oxygen-rich. This appears to be evidence against the idea that the HBB prevents luminous stars from becoming carbon stars by destroying dredged-up carbon through the CN cycle to produce an oxygen-rich environment. In this way, HBB has been viewed as the possible cause for the rarity of luminous carbon-rich stars. However, recent observational finding of luminous ($M_{\mathrm{bol}} \sim -7$) carbon-rich stars in the Magellanic Clouds by van Loon et al. (1998) suggests that HBB is only a part of a complicated mechanism operating during the AGB phase. Recently Frost et al. (1998) suggested that the chemistry of the photosphere, whether it is carbon-rich or oxygen-rich, depends on the efficiency of both the mass-loss and the third dredge-up during the AGB phase. They argue that if the minimum envelope mass required for third dredge-up is less than that for HBB, dredge-up continues even after the HBB ceases. This continuation of dredge-up after the cessation of HBB may be the explanation for the occurrence of luminous carbon stars. This would thus explain the high Li abundance and apparently high luminosity in a carbon-rich PPN like IRAS Z02229+6208.

The distance to IRAS 07430+1115 is unknown, since it does not have the series of foreground interstellar clouds to give us a good lower limit as was the case with IRAS Z02229+6208. Thus we do not know if it also has a high luminosity and mass as does IRAS Z02229+6208. However, high amounts of Li have also been observed in low-mass carbon-rich AGB stars (Abia et al. 1991) and the low-mass carbon-rich post-AGB star IRAS 05341+0852 (Reddy et al. 1997). The four Li-rich AGB stars studied by Abia et al. have $M_{\mathrm{bol}} \sim -6.2$ to -5.0. These are less luminous than the Li-rich AGB stars found in the SMC and indicate that Li overabundance can occur in the Galaxy in stars of lower luminosity and lower mass. The findings of Li in IRAS Z02229+6208 and IRAS 07430+1115, and also in the similar objects IRAS 22272+5435 and IRAS 05431+0852, suggest that these post-AGB stars are probably the successors of a rather small group of Li-rich and carbon-rich AGB stars. Note that not all of the carbon-rich PPNs display an overabundance of Li. If the dredge-up continues long after HBB ceases, it is expected that Li will be destroyed, which may explain the scarcity of carbon-rich AGB and post-AGB stars found to be Li-rich.

4.3. *Circumstellar Envelope*

We have detected the circumstellar envelopes in molecular absorption bands (C_2 and CN) and atomic absorption lines (Na I and K I). They had previously been detected in millimeter CO emission (Hrivnak & Kwok 1999).

Radial velocity studies of few similar carbon-rich PPNs have revealed radial velocity variations of $\sim$8 km s^{-1} (peak-to-peak) due to photospheric pulsations (Hrivnak & Lu 1999). In the cases of IRAS Z02229+6208 and IRAS 07430+1115, we find differences of $\sim$1–2 km s^{-1} between the velocity measurements of CO emission and the visible spectral lines (Table 2). This difference may be also due to pulsation of the photosphere. Assuming that the CO velocities represent the system velocities, we compare the expansion velocities derived from CO, C_2, CN, Na I, and K I features in Table 9. We find that these features all possess similar velocities, confirming that they are all formed in the circumstellar envelope. These values, 8–15 km s^{-1}, are typical of the expansion velocities observed in AGB stars and PPN envelopes.

The expansion velocities, rotational temperatures, and column densities of C_2 in the circumstellar shells surrounding IRAS Z02229+6208 and IRAS 07430+1115 are in the same range as those determined by Bakker et al. (1997) in other carbon-rich post-AGB stars. It is interesting to note that some of the molecular C_2 lines appear to show a P Cygni–shaped profile in the spectrum of IRAS 07430+1115 (Fig. 4). The presence of P Cygni profiles is not fully unexpected since the lines are formed in an expanding shell. C_2

TABLE 9

SUMMARY OF CIRCUMSTELLAR VELOCITY COMPONENTS

COMPONENT	Z02229+6208		07430+1115	
	V_r(km s^{-1})	V_{exp}(km s^{-1})	V_r(km s^{-1})	V_{exp}(km s^{-1})
Photosphere (atomic lines).....	18	...	35	...
System (CO).....	20	...	34	...
CSE (CO).....	...	15	...	15
CSE (C_2).....	6	14	23	11
CSE (CN).....	8	12	24	10
CSE (Na I).....	6	14	20	14
CSE (K I).....	9	11	26	8

emission has been seen previously in the visible spectrum of the carbon-rich PPN AFGL 2688 (Egg Nebula) by Cohen & Kuhi (1977). By means of spectropolarimetry, they have shown the presence of an underlying C_2 absorption component due to light from near the star, scattered by the lobes, and a C_2 emission component originating in the lobes. Hora & Latter (1994) have observed C_2 and CN emission in the near-infrared spectrum of AFGL 2688. Recently Klochkova et al. (1999) presented spectra of the carbon-rich PPN IRAS 04296+3429 which shows the C_2 band to be in emission. Thus, while C_2 emission does not appear to be common, IRAS 07430+1115 is one of a few PPNs in which it has been observed. In the case of IRAS 07430+1115, the P Cygni–like profile suggests that we may be seeing C_2 emission from portions of the circumstellar envelope that are not expanding toward us. It would be interesting to obtain high spatial resolution images of IRAS 07430+1115 to see if these would help one to understand the mechanism responsible for this sort of circumstellar C_2 profile.

5. SUMMARY AND CONCLUSIONS

From high-resolution spectroscopic analysis, we determined the following atmospheric models: $T_{\rm eff} = 5500$ K, $\log g = 0.5$, $\xi_t = 4.25$ km s^{-1}, and [M/H] = −0.5 for IRAS Z02229+6208, and $T_{\rm eff} = 6000$ K, $\log g = 1.0$, $\xi_t = 3.50$ km s^{-1}, and [M/H] = −0.5 for IRAS 07430+1115. The elemental abundance analyses show that both stars are metal-poor and overabundant in C, N, and *s*-process elements, which are the primary chemical characteristics of the post-AGB phase. Thus both stars are unambiguous post-AGB objects. The observed *s*-process elemental patterns for these two stars are similar to other PPNs studied recently by Reddy et al. (1997) and Decin et al. (1998). In common with these two studies, the derived value of the neutron exposure parameter ($\tau_0 \approx 0.2$) is found to be significantly less than that found for AGB stars. These results may lead to a better understanding of the nature of the thermally pulsating AGB phase.

In addition to C, N, and *s*-process enhancements, the spectrum synthesis analysis of the Li I doublet at 6707 Å shows an enhanced Li abundance, $\log \epsilon(\rm Li) = 2.3$ (IRAS Z02229+6208) and $\log \epsilon(\rm Li) = 2.4$ (IRAS 07430+1115). The overabundances of Li found in these stars are similar to those in two other carbon-rich PPN stars, IRAS 05341+0852 and IRAS 22272+5435, and suggests that these may be all descendents of a rare group of carbon-rich and Li-rich AGB stars.

The rotational temperatures, column densities, and expansion velocities derived from circumstellar C_2 and CN absorption lines are typical of the values found for post-AGB stars. IRAS 07430+1115 is unusual in that it shows an emission component in the C_2 lines. We found the use of high-resolution spectra of the Na I D lines to be a very important tool in studying the physical properties of PPNs. For IRAS Z02229+6208, which is in the Galactic plane, several additional velocity components were seen which are due to foreground interstellar clouds. These were used to set an important lower limit to the distance to the PPN. This was used to estimate lower limits to the luminosity and initial mass, which are important to our understanding of nucleosynthesis during the AGB phase. This technique can be used profitably for post-AGB stars near the Galactic plane.

We thank G. Gonzalez and H. Van Winckel for many useful suggestions and the referee, T. Kipper, for his suggestion which led us to a more careful examination of the K I lines. We have made extensive use of the NASA ADS data base. This research was supported by grants to B. J. H. from NASA (NAG 5-1223) and the NSF (AST 93-15107).

TABLE 10

ABUNDANCE RESULTS OF INDIVIDUAL LINES, BASED ON THE ADOPTED MODELS

			Z02229+6208		07430+1115	
λ (Å)	LEP (eV)	log *gf*	W_λ (mÅ)	log ϵ(X)	W_λ (mÅ)	log ϵ(X)
			Li I			
6707.7	0.00	…	65	2.3	40	2.4
			C I			
6587.62	8.53	−1.050	110	8.71	120	8.87
6655.51	8.54	−1.942	65	9.13	…	…
7087.83	8.65	−1.480	70	8.84	54	8.63
7100.13	8.64	−1.470	60	8.69	66	8.66
7108.92	7.95	−1.680	115	8.80	…	…
7111.48	8.64	−1.330	…	…	80	8.67
7113.17	8.64	−0.960	160	8.97	130	8.63
7115.17	8.64	−0.930	…	…	120	8.69
7116.96	8.65	−1.080	…	…	135	9.00
7119.70	8.64	−1.309	…	…	110	8.97
7476.18	8.77	−1.643	63	9.03	50	8.75
7685.20	8.77	−1.573	45	8.72	50	8.68
7840.25	8.85	−1.852	32	8.83	…	…
			[C]			
8727.13	1.26	−8.210	170	8.66	130	8.81
			N I			
7468.31	10.34	−0.130	62	8.67	40	8.02
8629.24	10.69	0.090	65	8.66	45	7.92
8680.28	10.34	0.420	125	8.67	…	…
8686.15	10.33	−0.270	65	8.68	40	7.90
9045.80	12.36	0.420	14	8.69	…	…
9392.66	10.69	0.328	…	…	70	8.02
			Mg I			
5711.10	4.34	−1.683	120	7.21	95	7.19
			Al I			
6696.03	3.14	−1.320	40	6.19	40	5.96
			Si I			
7405.79	5.61	−0.570	153	7.53	100	7.30
7932.35	5.96	−0.471	120	7.50	75	7.25
8742.47	5.87	−0.510	125	7.37	105	7.33
			S I			
8679.65	7.87	−0.460	65	7.05	65	6.97
8693.96	7.87	−0.560	60	7.09	60	7.00
			Ca I			
5261.71	2.52	−0.500	157	6.19	…	…
5512.99	2.93	−0.500	…	…	80	6.07
5601.29	2.52	−0.630	…	…	107	6.10
5590.13	2.52	−0.740	93	5.82	…	…
6166.44	2.52	−1.260	…	…	35	5.90
6449.81	2.52	−0.620	135	6.02	99	5.98
6455.60	2.52	−1.290	72	6.14	…	…
6471.67	2.52	−0.686	130	6.03	…	…
6493.79	2.52	−0.390	181	6.19	…	…
6499.65	2.52	−0.818	121	6.09	…	…
6717.69	2.71	−0.390	120	5.84	110	6.05

TABLE 10—*Continued*

			Z02229+6208		07430+1115	
λ (Å)	LEP (eV)	log *gf*	W_λ (mÅ)	log ϵ(X)	W_λ (mÅ)	log ϵ(X)
			Sc II			
6279.74	1.50	−1.280	170	2.70	108	2.60
6604.60	1.36	−1.230	175	2.51	140	2.68
			Ti II			
6559.58	2.05	−2.300	145	4.47	…	…
			Cr I			
7400.19	2.90	−0.080	100	5.39	55	5.26
			Cr II			
5407.62	3.83	−2.380	120	5.45	80	5.26
5502.09	4.17	−2.090	100	5.32	…	…
			Fe I			
5198.72	2.20	−2.189	143	6.86	…	…
5373.71	4.47	−0.880	…	…	50	7.19
5445.05	4.39	0.050	…	…	128	7.11
5701.56	2.56	−2.210	130	7.09	82	7.09
5763.00	4.21	−0.230	…	…	120	7.11
5862.37	4.55	−0.379	95	7.00	…	…
5984.83	4.73	−0.310	…	…	80	7.20
6003.02	3.88	−1.120	…	…	70	7.10
6008.57	3.88	−0.980	98	6.93	90	7.18
6024.07	4.55	−0.020	130	6.94	110	7.04
6065.49	2.61	−1.490	195	6.98	150	7.19
6213.44	2.22	−2.610	160	7.34	80	7.12
6215.15	4.19	−1.440	…	…	30	7.17
6219.29	2.20	−2.420	170	7.22	…	…
6322.69	2.58	−2.425	97	7.01	45	6.87
6335.34	2.20	−2.200	185	7.12	130	7.23
6336.83	3.69	−0.680	150	6.86	115	6.93
6408.03	3.69	−1.000	140	6.92	98	7.06
6411.66	3.65	−0.820	…	…	109	6.96
6421.36	2.28	−2.010	175	6.92	130	7.04
6609.12	2.56	−2.670	60	7.09	35	6.95
810.26	4.61	−1.120	35	6.89	…	…
7531.15	4.37	−0.590	103	7.12	85	7.17
7568.91	4.28	−0.990	75	7.01	50	7.06
7583.80	3.02	−1.960	115	7.07	…	…
7586.03	4.31	−0.180	170	7.07	112	6.95
7723.21	2.28	−3.590	25	7.10	…	…
7748.28	2.95	−1.740	110	6.99	…	…
7780.57	4.47	−0.090	140	6.73	120	7.09
			Fe II			
5627.50	3.39	−4.240	…	…	60	7.21
5991.38	3.15	−3.760	140	7.00	100	6.90
6084.10	3.20	−3.990	110	7.03	96	7.14
6369.46	2.89	−4.310	145	7.29	…	…
6416.93	3.89	−2.850	154	6.94	123	6.94
7222.40	3.89	−3.370	133	7.26	75	6.94
7224.46	3.89	−3.390	103	7.02	67	6.87

TABLE 10—*Continued*

			Z02229+6208		07430+1115	
λ (Å)	LEP (eV)	log *gf*	W_λ (mÅ)	log ϵ(X)	W_λ (mÅ)	log ϵ(X)
			Ni I			
6598.59	4.24	−1.020	13	5.83	…	…
6643.64	1.68	−2.010	145	5.69	104	5.85
6767.78	1.83	−1.890	115	5.48	100	5.83
6772.32	3.66	−1.070	48	5.95	…	…
7385.24	2.74	−2.070	32	5.76	…	…
7393.61	3.61	−0.040	182	6.02	120	5.89
7409.10	3.80	−0.150	140	5.96	…	…
7414.51	1.99	−2.440	69	5.78	45	5.93
7422.29	3.63	−0.140	155	5.90	110	5.78
7522.78	3.66	−0.560	90	5.81	63	5.86
7525.12	3.63	−0.690	85	5.87	53	5.85
7555.61	3.85	0.060	157	5.94	110	5.91
7574.04	3.83	−0.630	60	5.78	50	5.94
7727.62	3.68	−0.150	135	5.78	…	…
7788.94	1.95	−2.420	72	5.73	52	5.96
7797.59	3.90	−0.230	…	…	85	5.99
			Y I			
6687.57	0.50	−0.430	40	3.59	…	…
6793.63	0.57	−0.240	36	3.41		
			Y II			
5610.36	1.03	−2.910	170	3.78	…	…
6832.48	1.74	−1.939	…	…	130	3.54
7450.33	1.75	−1.430	300	3.95	…	…
7264.16	1.84	−1.502	…	…	200	3.89
			Zr II			
6346.48	2.41	−1.300	196	4.26	160	4.39
6677.92	2.42	−1.360	210	4.41	167	4.51
			La II			
5377.07	2.30	0.700	180	1.95	175	2.41
5863.72	0.93	−0.990	180	1.93	160	2.49
			Ce II			
5610.25	1.05	0.000	186	2.09	170	2.56
5330.56	0.87	−0.230	175	2.07	…	…
5512.06	1.01	0.200	…	…	165	2.27
5975.82	1.33	−0.320	112	2.06	110	2.48
6043.40	1.21	−0.170	160	2.14	140	2.50
			Pr II			
5219.03	0.79	−0.150	183	1.70	…	…
5322.82	0.48	−0.540	195	1.85	190	2.54
5509.11	0.48	−0.820	165	1.82	…	…

TABLE 10—*Continued*

			Z02229+6208		07430+1115	
λ (Å)	LEP (eV)	log *gf*	W_λ (mÅ)	log ϵ(X)	W_λ (mÅ)	log ϵ(X)
			Nd II			
5276.88	0.86	−0.710	185	2.40	…	…
5416.38	0.86	−1.010	145	2.32	116	2.59
5431.54	1.12	−0.290	200	2.37	183	2.88
5442.29	0.68	−0.610	185	2.07	160	2.48
5620.62	1.54	−0.070	175	2.35	155	2.83
5804.02	0.74	−0.660	…	…	185	2.97
6031.31	1.28	−0.420	180	2.40	150	2.72
6034.23	1.54	−0.400	145	2.37	130	2.75
6183.91	1.16	−1.340	77	2.36	…	…
6365.54	0.93	−1.410	135	2.62	…	…
			Sm II			
6731.89	1.17	−0.510	95	1.40	75	1.65
			Eu II			
6173.06	1.32	−0.276	100	0.85	…	…
6437.70	1.32	−0.200	100	0.76	55	0.47
			Gd II			
5733.89	1.37	−0.360	60	1.37	35	1.40

REFERENCES

Abia, C., Boffin, H. M. J., Isern, J., & Rebolo, R. 1991, A&A, 245, L1
Andersen, J., Gustafsson, B., & Lambert, D. L. 1984, A&A, 136, 75
Bakker, E. J. 1995, Ph.D. thesis, Universiteit Utrecht
Bakker, E. J., & Lambert, D. L. 1998, ApJ, 502, 417
Bakker, E. J., van Dishoeck, E. F., Waters, L. B. F. M., & Schoenmaker, T. 1997, A&A, 323, 469
Bakker, E. J., Waters, L. B. F. M., Lamers, H. J. G. L. M., Trams, N. R., & van der Wolf, F. L. A. 1996, A&A, 310, 893
Biémont, E., Hibbert, A., Godefroid, M., & Vaeck, N. 1993, ApJ, 412, 431
Böhm-Vitense, E. 1972, A&A, 17, 335
Bond, H. E. 1991, in IAU Symp. 145, Evolution of Stars: The Photospheric Abundance Connection, ed. G. Michaud, & A. V. Tutukov (Dordrecht: Kluwer), 341
Brown, J. A., Sneden, C., Lambert, D. L., & Dutchover, E., Jr. 1989, ApJS, 71, 293
Busso, M., Gallino, R., Lambert, D. L., Raiteri, C. M., & Smith, V. V. 1992, ApJ, 399, 218
Busso, M., et al. 1995, ApJ, 446, 775
Cameron, A. G. W., & Fowler, W. F. 1971, ApJ, 164, 111
Cohen, M., & Kuhi, L. V. 1977, ApJ, 213, 79
Cunha, K., Smith, V. V., & Lambert, D. L. 1995, ApJ, 452, 634
Decin, L., Van Winckel, H., Waelkens, C., & Bakker, E. J. 1998, A&A, 332, 928
Dinerstein, H. L., Sneden C., & Uglum, J. 1995, ApJ, 447, 262
Frost, C. A., Cannon, R. C., Lattanzio, J. C., Wood, P. R., & Forestini, M. 1998, A&A, 332, L17
Führ, J. R., Martin, G. A., & Wiese, W. L. 1988, J. Phys. Chem. Ref. Data, 17, Suppl. 4, 1
Gallino, R., Busso, M., Picchio, G., Raiteri, C. M., & Renzini, A. 1988, ApJ, 334, L45
García-Lario, P., Manchado, P., Pych, W., & Pottasch, S. R. 1997, A&AS, 126, 479
Giridhar, S., & Arellano Ferro, A. 1995, Rev. Mexicana Astron. Astrofis., 31, 23
Gonzalez, G., Lambert, D. L., & Giridhar, S. 1997, ApJ, 481, 452
Hibbert, A., Biémont, E., Godefroid, M., & Vaeck, N. 1991, A&AS, 88, 505
———. 1993, A&AS, 99, 179
Hollowell, D., & Iben, I. , Jr. 1989, ApJ, 340, 966
Hora, J. L., & Latter, W. B. 1994, ApJ, 437, 281
Hrivnak, B. J. 1995, ApJ, 438, 341
———. 1997, in IAU Symp. 180, Planetary Nebulae, ed. H. J. Habing & H. J. G. L. M. Lamers (Dordrecht: Kluwer), 303
Hrivnak, B. J., & Kwok, S. 1999, ApJ, 513, 869
Hrivnak, B. J., Kwok, S., & Volk, K. 1989, ApJ, 346, 265
Hrivnak, B. J., & Lu, W. 1999, in IAU Symp. 177, The Carbon Star Phenomenon, ed. R. Wing (Dordrecht: Kluwer), 293
Hrivnak, B. J., et al. 1999, in preparation
Iben, I., Jr. 1981, in Physical Processes in Red Giants, ed. I. Iben, Jr. & A. Renzini (Dordrecht: Kluwer), 3
Iben, I., Jr., & Renzini, A. 1982, ApJ, 259, L79
Kipper, T., Jorgensen, U. G., Klochkova, G. K., & Panchuk, V. E. 1996, A&A, 306, 489
Klochkova, V. G. 1995, MNRAS, 272, 710
Klochkova, V. G., Szczerba, R., Panchuk, V. E., & Volk, K. 1999, A&A, in press
Kurucz, R. L. 1993, CD-ROM 13 (Cambridge: SAO)
Kurucz, R. L., & Petrymann, E. 1975, A Table of Semiempirical *gf*-Values (SAO Spec. Rept. 362)
Kwok, S. 1993, ARA&A, 31, 63
Kwok, S., Hrivnak, B. J., & Geballe, T. R. 1995, ApJ, 454, 394
Kwok, S., Volk, K. M., & Hrivnak, B. J. 1989, ApJ, 345, L51
———. 1999, in IAU Symp. 191, Asymptotic Giant Branch Stars, ed. T. LeBertre, A. Lebre, & C. Waelkens (San Francisco: ASP), 297
Lambert, D. L. 1991, in IAU Symp. 145, Evolution of Stars: The Photospheric Abundance Connection, ed. G. Michaud & A. V. Tutukov (Dordrecht: Kluwer), 4
Lambert, D. L., Heath, J. E., Lemke, M., & Drake, J. 1996, ApJS, 103, 183
Lambert, D. L., Smith, V. V., & Heath, J. 1993, PASP, 105, 568
Lattanzio, J. C., Frost, C.A., Cannon, R., & Wood, P. 1997, in Advances in Stellar Evolution: Stellar Ecology, ed. R. T. Rood & A. Renzini (Cambridge: Cambridge Univ. Press), 130
Luck, R. E., & Bond, H. E. 1991, ApJS, 77, 515
Luck, R. E., Bond, H. E., & Lambert, D. L. 1990, ApJ, 357, 188
Luck, R. E., & Lambert, D. L. 1985, ApJ, 298, 782
Mauron, N., & Querci, F. 1990, A&AS, 86, 513
Malaney, R. A. 1987, Ap&SS, 137, 251
Moore, C. E., Minnaert, M. G. J., & Houtgast, J. 1966, The Solar Spectrum 2935 Å to 8770 Å (NBS Monograph 61) (Washington, DC: US Government Printing Office)
Omont, A., et al. 1995, ApJ, 454, 819
Parthasarathy, M., García-Lario, P., & Pottasch, S. R. 1992, A&A, 264, 159
Parthasarathy, M., & Pottasch, S. R. 1986, A&A, 154, L16
Plez, B., & Lambert, D. L. 1994, ApJ, 425, L101
Reddy, B. E., & Hrivnak, B. J. 1999, AJ, 117, 1834
Reddy, B. E., & Parthasarathy, M. 1996, AJ, 112, 2053
Reddy, B. E., Parthasarathy, M., Gonzalez, G., & Bakker, E. J. 1997, A&A, 328, 331
Sackmann, I.-J. & Boothroyd, A. I. 1992, ApJ, 392, L71
Smith, V. V., Cunha, K., Jorissen, A., & Boffin, H. M. J. 1996, A&A, 315, 179
Smith, V. V., & Lambert, D. L. 1989, ApJ, 345, L75
———. 1990, ApJ, 361, L69
Sneden, C. 1973, Ph.D. thesis, Univ. of Texas, Austin
Takeda, Y. 1991, A&A, 243, 455
Thévenin, F. 1989, A&AS, 77, 137
———. 1990, A&AS, 82, 179
Tull, R. G., MacQueen, P. J., Sneden, C., & Lambert, D. L. 1995, PASP, 107, 251
van Loon, J. Th., et al. 1998, A&A, 329, 169
Van Winckel, H. 1999, in IAU Symp. 191, Asymptotic Giant Branch Stars, ed. T. LeBertre, A. Lebre, & C. Waelkens (San Francisco: ASP), 465
Van Winckel, H., Mathis, J. S., & Waelkens, C. 1992, Nature, 356, 500
Van Winckel, H., Waelkens, C., & Waters, L. B. F. M. 1995, A&A, 293, L25
———. 1996, A&A, 306, L37
Venn, K. 1995, ApJ, 449, 839
Wilson, T. L., Johnston, K. J., & Mauersberger, R. 1991, A&A, 251, 220
Začs, L., Klochkova, V. G., & Panchuk, V. E. 1995, MNRAS, 275, 764